



ECGANCOVID: Efficient Conditional GAN Architecture for Covid-19 Disease Segmentation

Payman Hussein Hussan ^{*1,2}  , *Israa Hadi Ali* ¹  

¹College of Information Technology, Department of Software, University of Babylon, Babil, Iraq.

²Babylon Technical Institute, Al-Furat Al-Awsat Technical University, Kufa, Iraq.

*Corresponding Author.

Received 09/09/2023, Revised 07/01/2024, Accepted 09/01/2024, Published Online First 20/09/2024



© 2022 The Author(s). Published by College of Science for Women, University of Baghdad.

This is an open-access article distributed under the terms of the [Creative Commons Attribution 4.0 International License](https://creativecommons.org/licenses/by/4.0/), which permits unrestricted use, distribution, and reproduction in any medium, provided the original work is properly cited.

Abstract

Severe Acute Respiratory Syndrome Coronavirus 2 (SARS-CoV-2) poses a global threat, impacting millions worldwide. While automated detection of lung infections through Computed Tomography (CT) scans is a promising alternative, segmenting infected regions from CT slices remains challenging due to low-contrast infection boundaries and blurred appearances. To address this challenge, A deep-learning model called ECGANCOVID-Net is proposed for detection and identification of infected regions in chest CT images. Our model utilizes a semantic hierarchical segmenter to detect regions of lung infection caused by Coronavirus in CT medical images. The model consists of two components, namely the U-CGAN-Net models. The initial neural network, UCGAN-Net1, is designed to detect lung parenchyma. Subsequently, the second neural network, UCGAN-Net 2, operates on the segmented lungs to accurately identify the specific regions impacted by COVID-19 lesions. UCGAN-Net comprises a conditional generative adversarial network (CGAN) incorporating an adapted generator and discriminator. Furthermore, our model employs data augmentation techniques to address the issue of limited training data. Through extensive trials, it has been discovered that the suggested methodology exhibits superior performance compared to recently proposed techniques. This is particularly evident in the improved overall performance of our model when accurately determining the location of tiny lesions. The proposed ECGANCOVID net has demonstrated exceptional performance in segmenting COVID-19 lesions, achieving higher localization performance with a Dice Similarity Coefficient (DSC) of 84.5% and Intersection over Union (IOU). Additionally, the suggested model has undergone external validation using an unseen dataset, resulting in Dice Similarity Coefficient of 69.7%.

Keywords: COVID-19 disease, Computed tomography (CT) images, Conditional generative adversarial network (CGAN), Lung and lesion segmentation, Hierarchical segmentation strategy.

Introduction

The world is grappling with the challenge of COVID-19, a respiratory illness caused by the novel Coronavirus, significantly impacting various aspects of human life due to its highly contagious nature. As of August 8, 2021, there have been over 200 million confirmed cases and 4.25 million reported deaths worldwide, with the global infection rate continuing to rise.

Accurate diagnostic methods and efficient treatment protocols are imperative in addressing the ongoing pandemic. Various diagnostic techniques, including isothermal nucleic acid amplification technologies and real-time reverse transcription-polymerase chain reaction (RT-PCR), are available for identifying COVID-19. Currently, RT-PCR has become widely employed for COVID-19 diagnosis.

However, this method has limitations, including low Sensitivity, insufficient test kit availability, and suboptimal efficiency. Recent research suggests that chest computed tomography (CT) images may provide a viable alternative in healthcare due to their heightened Sensitivity, accuracy, and ease of accessibility¹.

The assessment of medical images is typically a laborious and time-intensive task performed by radiologists. While improvements in CT scan resolution and the number of slices have increased Sensitivity and accuracy, they have also resulted in elevated workloads. Clinical decision support systems relying on automated interpretation of medical images, particularly through artificial intelligence and deep learning models, have shown notable progress. Image segmentation, a sub-field garnering significant attention, aims to automate finding and labeling areas of interest within medical images, including organs and abnormalities. The application of neural networks in medical image segmentation has demonstrated strong predictive ability comparable to radiologists' performance. Implementing an automatic segmentation tool for Corona-infected regions can serve as a valuable clinical decision support system for physicians. Image segmentation plays a crucial role in assisting radiologists with diagnosis, disease monitoring, inspection processes streamlining, and accuracy enhancement by automatically highlighting abnormal features and regions of interest (ROIs)².

CT scans have the potential to detect incipient lesions and can be employed by radiologists for diagnostic purposes. The initial stage in evaluating lung illnesses via medical imaging involves lung segmentation. Accurate segmentation of COVID-19-related diseases from CT imaging is essential for analysis and quantification. Researchers have proposed various techniques for lung segmentation, categorized into handcrafted strategies and deep-learning approaches. Handcrafted techniques, such as morphological-based techniques³ and active contour models⁴, involve physician intervention, are subject to bias, and are time-intensive. Furthermore, manually designed segmentation techniques are often tailored to specific imaging modalities, applications, and datasets, posing challenges in generalizing across diverse scenarios. There is a pressing need for automated segmentation of lung infections caused by COVID-19 in healthcare settings.

Before the advent of Deep Learning (DL), conventional Medical Imagery (MI) segmentation techniques primarily relied on methods like active contour models⁴, level set-based approaches⁵, watershed algorithms⁶, region growing⁷, Markov Random Fields⁸, and their respective extensions. However, these methodologies produced satisfactory outcomes only when a significant contrast existed between the background and the object area. Models often incorporated local feature limitations and curvature constraints to enhance segmentation accuracy. Nevertheless, such solutions proved less effective in cases where the object and background areas exhibited identical characteristics. Therefore, using deep learning algorithms for addressing medical image segmentation presents a promising area of research with both theoretical and practical implications.

Deep learning approaches aim to assist in rapidly and precisely identifying abnormalities in radiographic pictures. However, for deep learning models to achieve effective generalization, they require extensive training with substantial data. The data must be adequately labeled, especially in tasks such as image segmentation. The research community widely acknowledges that convolutional neural network (CNN) based designs are the most promising and extensively used method currently available.

In medical imagery segmentation, convolutional neural networks have shown promising results lately. The Fully Convolutional Networks (FCN)⁹ model is frequently employed in contemporary medical image segmentation tasks based on information from CNN. Subsequently, using semantic segmentation or pixel-wise classification algorithms, novel techniques were suggested to enhance the accuracy of segmenting contaminated areas in radiographic scans. The encoder-decoder architecture, frequently utilized for semantic segmentation, incorporates methodologies such as the fully convolutional network (FCN). Within this architectural framework, the encoder module captures feature representations of the input data.

On the other hand, the decoder module utilizes these representations to restore location information that may have been lost during the pooling process, ultimately generating a binary mask. An exemplary instance of this architectural design is Unet, renowned for preserving essential information from input pictures by using skip connections between the encoding and decoding layers. The U-Net¹⁰

architecture, built with the help of Convolutional Neural Network (CNN), is modified to achieve better segmentation in the medical imaging domain. Various UNet-based models, such as the Attention Unet¹¹ and Residual Unet¹², have been specifically developed to effectively segment infections for COVID-19 purposes.

Generative Adversarial Networks (GANs) have recently presented an alternative approach to enhancing medical image segmentation and obtaining more precise outcomes, remaining a topic of active research. GANs have notably improved

Related works

Recently, numerous studies have proposed Machine Learning approaches to automate COVID-19 detection as a classification problem based on biomarker analysis, such as demographic and clinical information. These approaches provide discriminative semantic features for frameworks aiming at the early detection of this novel virus. Predicting newly contaminated and recovered COVID-19 cases is crucial for controlling disease progression. In a study¹⁵, the authors utilized machine learning and laboratory data to predict COVID-19 patients, comparing three DL methods: Support Vector Machines (SVM), artificial neural networks (ANN), and K-nearest neighbors (k-NN) algorithms. Models were verified with 10-fold cross-validation and train-test split methods using 18 laboratory data from 600 patients. The results indicated that SVM outperformed the other algorithms in accuracy. Another studies¹⁶⁻¹⁸, based on levels of lymphocytes, CRP, and SPO2, employed machine learning, using a Lasso-logistic regression model to forecast the risk level of patients with COVID-19. This research utilized data collected from Azizia Primary Healthcare Sector- Wasit Governorate-Iraq, predicting multi-class case severity (severe, moderate, and mild) with over 85% accuracy. This allows for early intervention, diagnosis, and potentially a reduction in mortality for COVID-19 afflicted individuals. Tackling the multitude of challenges posed by COVID-19, strategies to triage patients could aid in determining treatment priority and administering targeted medication to individuals at high risk of severe illness. Establishing a Multidimensional Examination Framework (MEF), the study authors¹⁷ prioritized severe COVID-19 patients using integrated multi-criteria decision-making (MCDM) methodologies. The MEF considered various

semantic medical image segmentation quality thanks to their exceptional synthesizing capabilities and potential to extract and distribute data effectively. The utilization of adversarial loss during training has been discovered to enhance semantic segmentation performance¹³. Image generation models, such as Generative Adversarial Networks (GANs)¹⁴, are increasingly used for various tasks, and Conditional GANs are utilized to generate images from existing ones by incorporating random noise, which is beneficial for style transfer.

dimensions of examination factors, including demographic information, laboratory findings, vital signs, symptoms, and chronic illnesses, to prioritize severe COVID-19 patients.

However, these studies face challenges, as clinical features alone may not always be adequate for detecting and assessing COVID-19 due to factors such as atypical presentations and overlapping symptoms with other respiratory diseases. Clinical signs alone may make it difficult to differentiate COVID-19 from similar illnesses. On the other hand, CT imaging provides a detailed view of lung abnormalities associated with COVID-19, offering valuable information to monitor changes in lung health over time. Ground-glass opacities, consolidation, and specific lung features are better visualized through CT scans.

Recent literatures¹⁹⁻²¹ have introduced various diagnostic approaches for automated COVID-19 diagnosis, emphasizing CNN-based classification models. In response to the challenge of choosing the most effective deep learning model for COVID-19 diagnosis, a study²² introduced a comprehensive approach using a unique crow swarm optimization methodology. This methodology aids healthcare administrators in selecting and evaluating the most effective COVID-19 diagnosis models based on deep learning. Previous studies focused on detecting and classifying Coronavirus without accurately identifying and localizing specific lesion areas in a particular radiographic image.

Conversely, the semantic segmentation networks exhibit strong performance in identifying regions affected by Coronavirus in each radiographic image. Nevertheless, utilizing pixel-level annotated ground truths is important to effectively train and validate these segmentation networks²³. Data annotation in the healthcare field necessitates the involvement of

skilled healthcare practitioners, along with a substantial allocation of time and resources. Medical image segmentation aims to precisely delineate regions of interest (ROIs) in medical images, such as organs or pathological anomalies, by assigning a label to each pixel. Segmentation is an essential process, particularly in the analysis of COVID-19 images, as it can assist radiologists in diagnosing the disease, monitoring its course, and enhancing the speed and efficiency of their work²⁴⁻²⁶. Several effective pixel-wise classification methods utilizing deep learning have been developed to aid in the swift and accurate diagnosis of Corona using medical imaging. For instance, Reference²⁷ devised a comprehensive network structure to semantically segment images. Reference²⁸ proposed a sophisticated deep-learning model called VB-Net for accurately segmenting lung infections and lungs from CT images of a patient with COVID-19. Reference²⁹ introduced a multi-task deep-learning framework that utilizes CT imaging to accurately differentiate lung infections.

Study³⁰ introduced COVID-SegNet, incorporating a feature variation block and progressive atrous convolutions to emphasize the different infected regions and their boundaries. The proposed method attained a DSC of 73% for the segmentation of Coronavirus. In addition, The researchers in study³¹ devised a method for object recognition that utilizes bounding boxes to emphasize the contaminated area. They employed a weakly supervised methodology to enhance the Model's performance using a restricted number of labeled Coronavirus samples and utilized different variations of the VGG model to categorize Corona cases from community-acquired pneumonia (CAP) and cases without pneumonia. A segmentation method based on image enhancement to highlight coronavirus-infected lung areas is presented in³². While extracting lung areas, each lung is separated and subjected to local contrast enhancement. This technique enhances the contrast in the lung images, resulting in more detailed information about the target regions.

Consequently, this leads to improved segmentation outcomes. Authors³³ introduced the Inf-Net, a deep neural network designed to segment lung infections caused by COVID-19. The network specifically targets areas with ground glass opacities and consolidation. The study authors³⁴ recently introduced a more advanced encoder-decoder design called the PCPLP network. The Model is enhanced using an upgraded attention strategy and a multiscale

multi-level feature recursive aggregation module to achieve more precise segmentation results. This module effectively learns global feature representations that pertain to lesion areas. The authors obtained favorable outcomes, with a dice coefficient of 78%, surpassing previous cutting-edge models. Expert radiologists can deliver more accurate and dependable localization through ground-truth infection masks. Thus, Degerli et al.³⁵ introduced an innovative method to create a map of COVID-19 infections. They accomplished this by assembling a collection of 2951 CXR images that included accurately labeled infection segmentation masks. Multiple encode-decoder convolutional neural networks were trained and assessed using the generated dataset. The highest-performing network acquired an F1 score of 86% for localized infections.

Nevertheless, their suggested methodologies are solely focused on localizing COVID-19 infections and fail to provide effective and accurately localized information regarding the affected areas in the CT scan of the lungs because the infection regions have ambiguous boundaries, complicating the detection of their presence. In addition to Coronavirus detection, the localization of infection is another vital task that aids in assessing the patient's condition and determining the treatment strategy. Additionally, numerous authors emphasize that the absence of extensive and specific datasets containing images of illnesses significantly complicates the task of training a model. Added to this is the intricate and time-consuming process of annotating each image. Only highly skilled medical personnel can perform this procedure, which significantly restricts the quantity of data that may be produced within a short timeframe. In this study, the aim is to overcome the limitations of previous research and create a model that can accurately detect COVID-19-associated findings in chest CT images in a targeted and efficient manner.

Motivation

While the studies mentioned above have shown encouraging outcomes in utilizing chest CT for COVID-19 diagnosis, there is still scope for enhancement, specifically in lesion segmentation. This improvement can benefit physicians in accurately diagnosing COVID-19 and evaluating the effectiveness of treatment. Previous research has focused on the segmentation of lungs and lesions, as mentioned above. Nevertheless, the efficacy of the lesion segmentation models remains low compared

to lung segmentation. Furthermore, these methods fail to offer efficient and accurately localized information regarding the infected regions in the CT scan of the lungs.

Therefore, to develop a high-performance method for the efficient and well-localized detection of COVID-19-related findings in chest CT images, the following questions are addressed: How can deep learning methodologies be enhanced to mitigate the impact of image resolution issues, particularly when dealing with CT scans where the appearance of organ tissues may lead to the mixing of categories of pixels? What approach could be employed to improve the delineation of boundaries between the surrounding normal tissues and infected areas in the lung, and what adaptations can be made to detect small affected areas? What innovative strategy can overcome the constraints posed by limited access to extensive datasets in areas such as medical image processing, for example, the absence of comprehensive COVID-19 datasets since early 2020? Due to the sensitive nature of patient health data, strict regulations and ethical considerations often restrict sharing and access to this information.

This paper aims to answer the above questions, which are significant for COVID-19 lesion segmentation. The contributions are as follows:

- 1- Proposing a deep learning hierarchical approach, ECGANCOVID, which utilizes two UCGAN-Nets to effectively segregate areas infected with the Coronavirus using C.T. scans. Our hierarchical approach mitigates irrelevant background interference by generating lung

Materials and Methods

To address the complex challenge of effectively identifying coronavirus-infected regions in CT scans, it is crucial to recognize that information outside the lungs is irrelevant, as the infected areas are within the lungs. Therefore, our proposed approach utilizes a hierarchical segmentation strategy instead of a direct segmentation approach. In

contour maps, addressing the issue where the appearance of other organ tissues in the CT scan may lead to the mixing of pixel categories.

- 2- To effectively handle the issue of significant infection variations and low-contrast boundaries for segmenting infectious regions from the lungs, A context-aware conditional generative adversarial network denoted by (CGAN) with an adapted architecture for the Generator and Discriminator is suggested.
- 3- Our designed Model successfully achieves robust segmentation of small lesions in chest C.T. images, performing superiorly to the latest deep segmentation networks by utilizing the strength of grouped L1 loss and PatchGAN discriminator loss functions, contributing to successfully capturing small regions.
- 4- The performance of ECGANCOVID-net is improved using an augmentation strategy, leveraging a large number of CT images to augment the training dataset effectively.

The remaining sections of the paper are structured in the following manner: In Section 2, our proposed pipeline has been presented, covering details on datasets, pre-processing methods, the architecture of the proposed ECGANCOVID-NET, and evaluation approaches. The experiments and evaluation metrics are discussed in Section 3. Section 4, the outcomes of our ablation study had been presented, conducts a comprehensive set of comparison assessments across the utilized baseline networks, and thoroughly discusses and analyzes the obtained results. Finally, in Section 5, our conclusions and future work are outlined.

direct segmentation, a CT scan slice is taken as input, and during the pre-processing phase, the chest CT photographs are scaled and normalized before being fed into the infection segmentation network. The output of this process is the COVID lesion segmentation.

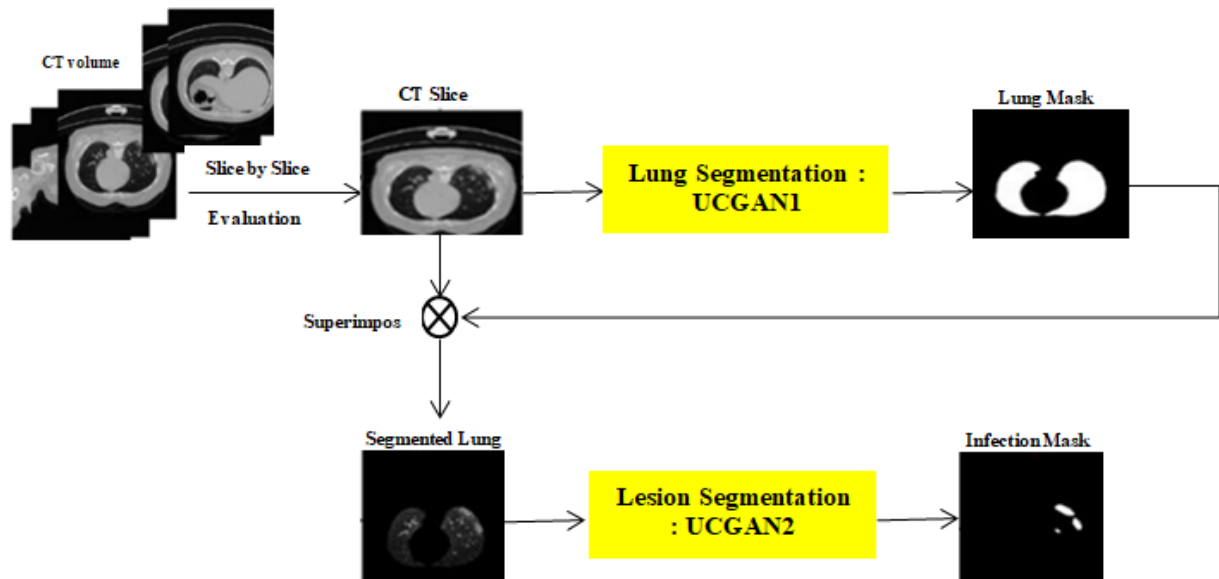


Figure 1. Structure of ECGANCOVID Network

Our COVID-19 hierarchical segmentation network, named ECGANCOVID-Net (depicted in Fig. 1), is developed based on Conditional Generative Adversarial Networks (CGAN) with an adapted architecture for the Generator and Discriminator and is employed to segment Coronavirus lesions from CT images in this study. The input CT volumes are analyzed slice by slice to identify the COVID-19-infected regions. Two UCGAN-Net models (UCGAN-Net1 and UCGAN-Net2 in Fig. 1) are connected in series to perform hierarchical segmentation.

The primary task of these UCGAN-Net models is semantic segmentation, classifying each pixel of the input CT image as either black '0' or white '1'. The output of UCGAN-Net1 indicates the presence of the "lung region" with white pixels ('1') and the

"background" with black pixels ('0'). Similarly, the output of UCGAN-Net2 represents the "infectious region" and "normal/background region" using white pixels ('1') and black pixels ('0'), respectively.

For each input CT slice, a binary lung mask is produced by the first UCGAN-Net1. Subsequently, the lung is segmented based on the created mask, and the results are input into the second UCGAN-Net2, which identifies the infected lung areas. The segmented lung mask is generated by superimposed (intersection) of the grayscale image with the binary lung mask. Fig. 2 displays several instances of lung segmentation in slices affected by COVID-19 infection. Finally, COVID-19 pneumonia lesions can be localized using the infection masks and lung masks that have been generated.

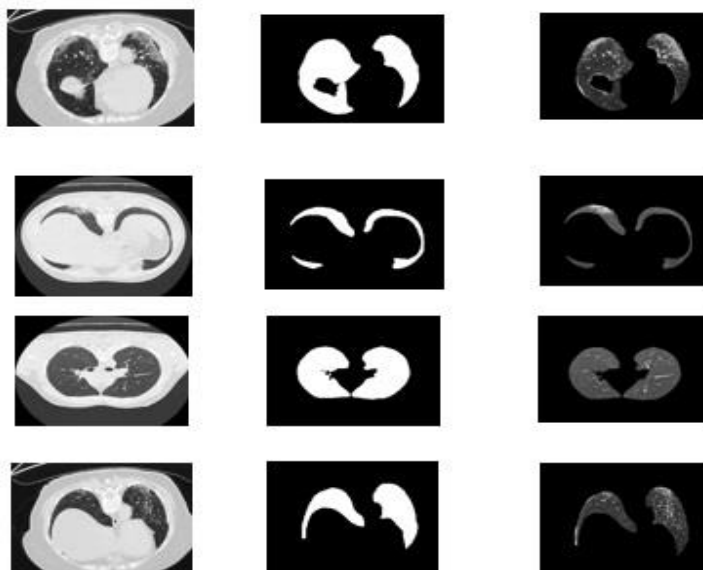


Figure 2. illustrates visual representations of lung segmentation. The initial column presents the input C.T. scan slice; the second column showcases the output of the lung mask, and the final column illustrates the results of lung segmented images after masking the lung mask with corresponding raw images.

Dataset Description

The present study used two publically available datasets, namely the COVID-19 CT Lung and Infection Segmentation Dataset³⁶ and the COVID-19 CT Segmentation Dataset³⁷, to train and assess the proposed system. The dataset used for the C.T. photographs segmentation modeling procedure, including the training and testing phases, is specifically sourced from the lung CT-scan dataset referenced in³⁶. The dataset collected by Ma et al. has a total of 20 chest C.T. volumes that have been annotated for COVID-19. All cases were confirmed Corona infections, with the proportion of individuals exhibiting lung infection ranging from 0.01% to 59%³⁸. The CT scans include a total of 3520 slices and have been sourced from approved sources such as Radiopaedia³⁹ and the Corona-Cases Initiative (RAIOSS)⁴⁰. Additionally, to provide C.T. scan files, reference³⁶ includes two masks intended for segmentation. The

lung mask and the infection mask are the two types of masks. The dataset was subjected to manual annotation by two radiologists and later validated by an experienced radiologist. Table 1 awards a full summary of the dataset employed to analyze C.T. scans. The dataset comprises C.T. scans with varied width and height dimensions and Depth represented by slices. Subsequently, the scans are scaled to a standardized size of $256 \times 256 \times 1$. The provided class labels for each pixel in the slices indicate whether it pertains to the region of interest. A pixel assigned with a label of 1 indicates its association with the lungs in the lungs annotation and with COVID-19, notably ground-glass opacities and consolidations, in the infection annotation. In contrast, a label value of 0 signifies that the pixel corresponds to the background. Table 2 displays a comprehensive profile of the C.T. scan utilized for each patient.

Table 1. Four samples (patient 1, patient 5, patient 10, and 19) were from the dataset ³⁶


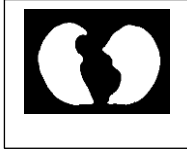



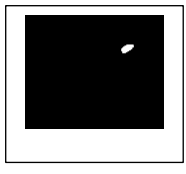
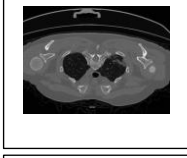
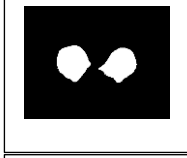


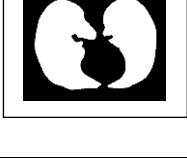

C.T. scan slice	Lung mask	Infection mask
		
		
		
		

Table 2. The source and size information of the C.T. scans for each patient.

Patient	Source	Size(width x height x Depth)
Patient1	Raioss	512 x 512 x 301
Patient2	Raioss	512 x 512 x 200
Patient3	Raioss	512 x 512 x 200
Patient4	Raioss	512 x 512 x 270
Patient5	Raioss	512 x 512 x 290
Patient6	Raioss	512 x 512 x 213
Patient7	Raioss	512 x 512 x 249
Patient8	Raioss	512 x 512 x 301
Patient9	Raioss	512 x 512 x 256
Patient10	Raioss	512 x 512 x 301
Patient11	Radiopaedia	630 x 630 x 39
Patient12	Radiopaedia	630 x 630 x 45
Patient13	Radiopaedia	630 x 630 x 39
Patient14	Radiopaedia	630 x 630 x 418
Patient15	Radiopaedia	630 x 401 x 110
Patient16	Radiopaedia	630 x 630 x 66
Patient17	Radiopaedia	630 x 630 x 42
Patient18	Radiopaedia	630 x 630 x 42
Patient19	Radiopaedia	630 x 630 x 45
Patient20	Radiopaedia	630 x 630 x 93


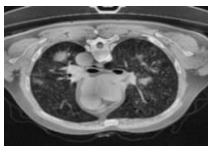

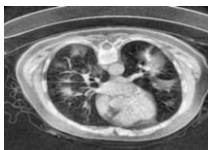
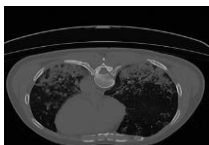
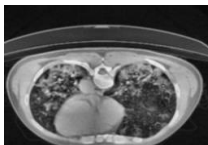
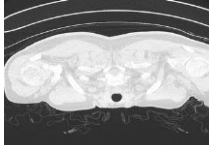
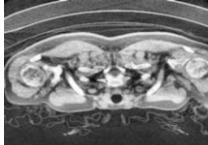
The second dataset was used for testing and evaluating the proposed ECGANCOVID model called COVID-19 CT segmentation dataset³⁷ comprises nine patients, with a total of 829 slices, where Each slice has dimensions of $630 \times 630 \times d^*$, where d^* denotes that the number of slices is different for each volume.

Pre-processing

To improve the quality of C.T. photographs and highlight their properties, the CLAHE⁴¹ "Contrast Limited Adaptive Histogram Equalisation" method is utilized for tackling contrast concerns such as noise and intensity inhomogeneity. This technique was utilized to improve the contrast of the acquired images and it is a variation of Adaptive Histogram Equalisation (AHE)⁴². The main goal of the CLAHE technique is to determine the mapping for each pixel by examining the grayscale

distribution in its surrounding area. This is accomplished using a transformation function that minimizes contrast amplification in densely populated areas. The efficacy of (CLAHE) in allocating displayed intensity levels in chest C.T. scans has been demonstrated in previous studies^{42,43}. By implementing this methodology, identifying the COVID-19 infection area within a C.T. image is improved, making it more distinguishable. Table 3 compares the CT-scan slices before and after implementing CLAHE. All datasets utilized for this investigation had photos in the neuroimaging informatics technology initiative (NITI) format. The format of all images had been changed to PNG and normalized the pixel values to fall within the range of 0–255 to limit the present variability. For the segmentation tasks, the final step was to resize all of the photos from the three different datasets to 256 by 256.

Table 3. Comparison of CT-scan images before and after applying Contrast Limited Adaptive Histogram Equalization (CLAHE) pre-processing.

Without CLAHE	With CLAHE
	
	
	
	

Data Augmentation

Due to the scarcity of annotated medical images and to improve the generalization capabilities of our models while reducing overfitting, data augmentation techniques have been implemented in our training sets. This study employed data augmentation techniques, including horizontal flipping⁴⁴, to generate more images with lesions.

Horizontal flipping, as a geometric transformation in image data augmentation, refers to mirroring an image horizontally. It involves flipping an image across a vertical axis, creating a mirror image of the original by reversing the left and right sides. This technique is part of the fundamental data manipulation methods used to enhance datasets. In horizontal flipping, Data augmentation is

implemented for each slice in the training set to generate more samples by the original image flipped or mirrored left to right, generating a new image that is the horizontal reflection of the initial image. Following the implementation of data augmentation techniques, the training set has been expanded to include total slices. Similarly, the test set now comprises 1001 CT slices. The data set's size grew around 83.6% and 83.5% for the training and test sets, respectively.

Proposed Network Architecture for Segmentation of the Lung and Lesions

The Generative Adversarial Network (GAN) model¹³, initially proposed by Goodfellow et al. In 2014, it was extensively utilized in image processing. These models are employed to transform input images into their corresponding output images. The GAN framework comprises two separate networks: a generator and a discriminator. The Generator is responsible for synthesizing high-fidelity images, while the Discriminator's role is to differentiate between synthetic and authentic photos from the training dataset, classifying them as either fake or real. The methodology employed entails the utilization of a min-max strategy by Generator G in conjunction with the Discriminator. The goal is to transform a collection of noise samples, denoted as z , that follow the distribution into actual data that aligns with the distribution. p_{data} . During the training phase, the discriminator network aims to distinguish between actual data samples y , which follow the probability distribution. p_y , and modified data samples $G(z)$, which conform to the distribution p_{data} . The mathematical representation of the objective function for the min-max GAN is as follows:

$$\min_G \max_D L_{GAN}(G, D) = \min_G \max_D E_{y \sim p_y} [\log D(y)] + E_{z \sim p_z} [\log(1 - D(G(z)))] \quad 1$$

The symbols E and \log represent the mathematical operations of expectation and logarithm. The previous output of the Generative Adversarial Network demonstrates a notable level of ambiguity,

which prevents its ability to generate the desired objects. In 2014, Mirza and colleagues proposed using Conditional Generative Adversarial Nets (CGAN)¹⁴ as a potential solution to a specific problem. This approach involves the generation of output data x using a generator G , which utilizes real data y and a random noise vector z . The given expression can be $G: \{y, z\} \rightarrow x$. Meanwhile, the Discriminator of CGAN, referred to as D , takes the generated and real data (x and y) as inputs and aims to distinguish between them. The mathematical formulation of the objective function for Conditional Generative Adversarial Networks (C-GAN) is as follows:

$$L_{CGAN}(G, D) = E_{x \sim p_x, y \sim p_y} [\log D(x, y)] + E_{y \sim p_y, z \sim p_z} [\log(1 - D(y, G(y, z)))] \quad 2$$

The Conditional Generative Adversarial Network (CGAN) technique is used in the current study to segment the lung and lesions in COVID-19. The CT scans are input for the Generator, designed to produce a corresponding lung mask depending on the predicted outcome. The Discriminator accepts two sets of inputs: the actual pair (the original chest C.T. scan and its related ground truth lung mask) and the fake pair (the original chest C.T. scan and the synthesized lung mask). The training method for the Generator and Discriminator is adversarial, as illustrated in Fig. 3. The Generator tries to fool the Discriminator by generating progressively realistic images of a lung mask. At the same time, the Discriminator attempts to distinguish between genuine and fake photos. The Generator, denoted by G , takes an input image of a chest C.T. scan, denoted by y , and produces a synthesized segmented mask image, denoted by $G(y)$. At the same time, The Discriminator indicated that D 's primary aim is to distinguish between two sets of photographs. The first set consists of a synthetic picture (y) and a ground truth mask image, whereas the second set consists of a synthetic image (y) and a generated image ($G(y)$).

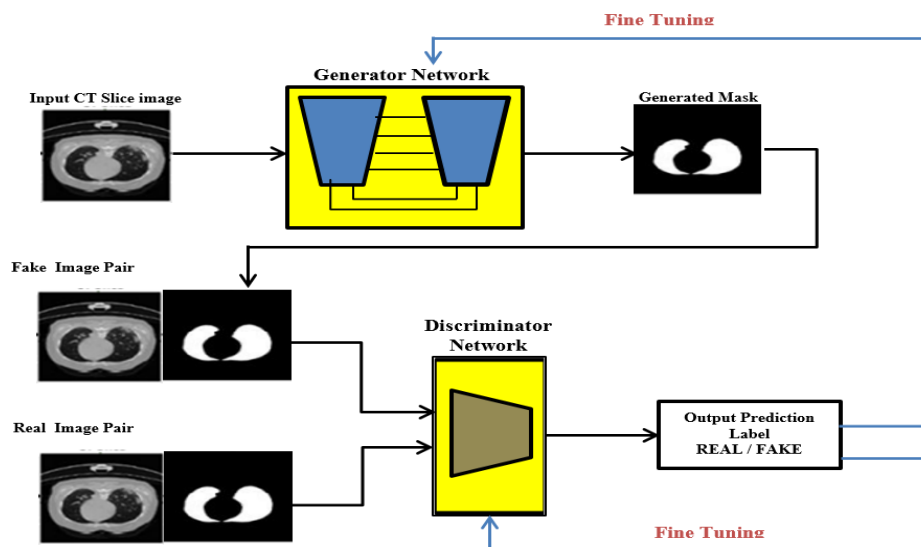


Figure 3. Structure of the Conditional Generative Adversarial Network for segmentation of lungs (training phase)

Our proposed network, UCGAN-net, is designed to accurately segment the lung's affected region from C.T. images. This segmentation is achieved by utilizing Conditional Generative Adversarial Networks (CGAN) with an adapted architecture for the Generator and Discriminator. The generative network learns the ability to identify our Region of Interest (ROI) and generates a binary mask that precisely delineates its boundaries. On the other hand, the Discriminator learns the ability to distinguish between authentic segmented masks and artificial ones. Our proposed CGAN architecture (UCGAN-net) is inspired by Unet¹⁰ and the PatchGAN⁴⁵ models focusing on convolutional layers for extracting low and high-level features from input images, where the proposed deeper a U-Net has been used instead of an autoencoder as the Generator's backbone to preserve low-level and textural information also, the Discriminator has been changed to Patch-GAN capable of handling large images based on the fixed-size patch discriminator.

Generator Network with skip connection:

The research employed a convolutional encoder-decoder architecture for the generator network, which resembles Unet¹⁰ and allows it to perform style transfer based on paired training images while preserving the pixel-wise characteristics of the source image by combining high-level semantic and detailed pixel information.

The generator structure consists of three primary components: the encoder, the bottleneck, and the

decoder. To enhance the accuracy of UNet in generating segmentation maps, our Generator has been improved by augmenting the number of layers in the encoder. Specifically, an encoding section that adheres to the conventional architecture of convolutional neural networks, consisting of seven encoder blocks instead of the original four blocks in the Unet¹⁰ architecture, has been incorporated. Every encoder block processes an input image by applying a single convolutional layer, followed by batch normalization and a leaky rectified linear unit with a slope of 0.2. In contrast to the original UNet, all max-pooling layers have been eliminated. After each block, the kernels are doubled by two to enhance the architecture's ability to effectively learn complex structures. The bottleneck part serves as the intermediary between the contraction and expansion layers. Its structure consists of a single 4x4 convolutional layer with a stride of 2x2, which is then followed by a ReLU activation layer. These connections are commonly known as skip connections. The expansion part, similar to the contraction section, consists of seven blocks. Within each decoder block, the input image undergoes a sequence of operations: a deconvolutional layer, batch normalization, a dropout layer, concatenation, and an activation layer. In our suggested Model, various techniques are employed, such as batch normalization and dropout, to mitigate the issue of overfitting. In contrast to the encoder blocks, the number of feature maps is halved to preserve symmetry. The input for the relevant contraction layer is concatenated in the concatenate layer. This

guarantees that the captured features during the contraction phase are utilized to reconstruct the new image.

The number of encoder blocks corresponds to the number of decoder blocks. Subsequently, the output from the expansion block is sent into another deconvolutional layer, which adjusts the number of feature maps to match the desired number of segments or classes. The convolutional and deconvolutional layers both employ a 4x4 kernel and a 2x2 stride, resulting in the reduction and expansion of the feature maps, respectively. Fig. 4 depicts this architecture. Using the deeper UNet architecture in the Generator of UCGAN NET provides several benefits. One key advantage is its ability to handle large amounts of spatial information, making it well-

suiting for medical image segmentation tasks where the input images can be very large.

Additionally, the symmetrical architecture of the U-Net enables the efficient transfer of information from the down-sampling path to the up-sampling path, preserving fine details such as texture and object boundaries, of the segmentation mask. The U-Net also includes skip connections, which are implemented by concatenating activation from an earlier layer to the activation of a deeper layer. This allows the network to access high-level and low-level features, providing a complete representation of the input image. The skip connections also help capture long-range dependencies in the data by combining features from the contracting path with those from the expanding path.

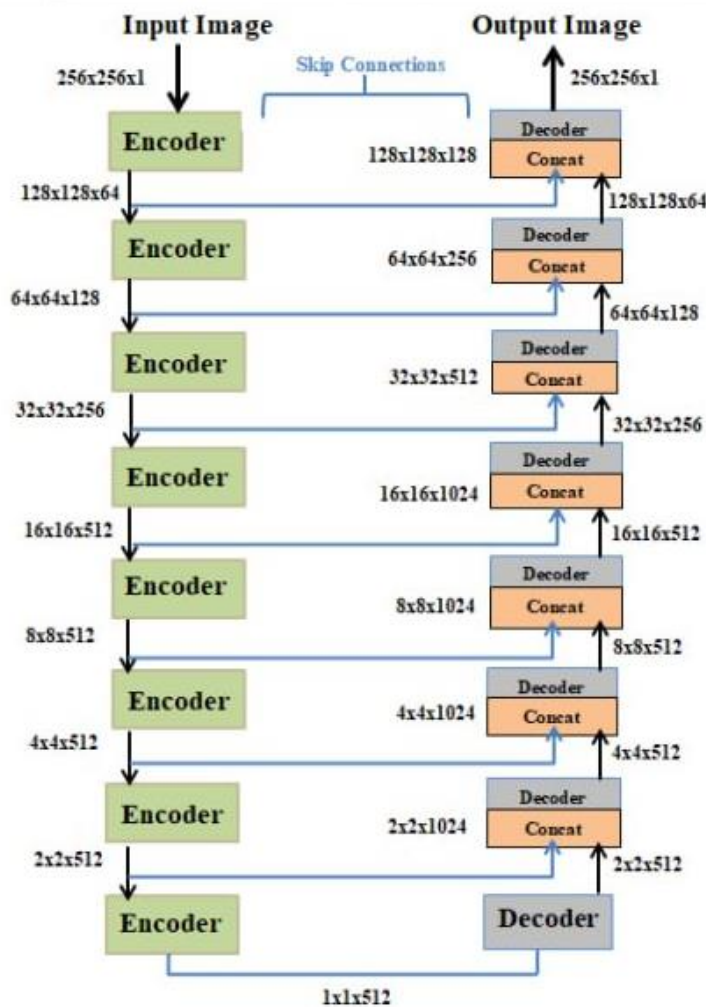


Figure 4. The architectural diagram shows the generator network utilized within the UCGAN framework.

Discriminator Network:

The Discriminator evaluates the authenticity of a given binary mask by determining whether it is real or generated. Specifically, the employed Discriminator in this study is referred to as a Patch-GAN⁴⁵, which partitions the input image into a collection of patches and assigns a single scalar output to each Patch. Unlike a traditional image discriminator that predicts the full image, a patch discriminator predicts each Patch and the final prediction is obtained by averaging all the patch predictions. Additionally, our patch discriminator requires fewer parameters, demonstrates robust performance with large and blurry images, and has a shorter computational time. Our Model utilizes a patch discriminator with a patch size of 70x70 pixels, resulting in the highest image sharpness in both spatial and spectral domains. The implemented Model takes two input images that are concatenated, and Gaussian noise with a standard deviation of 0.2 is introduced to the concatenated input before

entering the initial hidden layer to mitigate overfitting. The structure of our Discriminator includes three hidden layers, followed by batch normalization and leaky ReLU. The convolutional layers consist of filters with dimensions of 4x4 and a stride of 2x2. Furthermore, the Discriminator is subjected to regularization by imposing constraints on the magnitudes of its gradients through the utilization of L1 regularization. Hence, an L1 regularizer is incorporated into every convolutional layer.

The final block within the Discriminator produces a patch of dimensions 30x30x1, wherein each pixel of this Patch serves to classify a distinct section of the input image. The Leaky Rectified Linear Unit (ReLU) is frequently utilized as an activation function in all layers. Except for the last layer, it is substituted with a sigmoid function. Fig. 5 presents an architectural schematic depicting the discriminator network employed in the UCGAN Net.

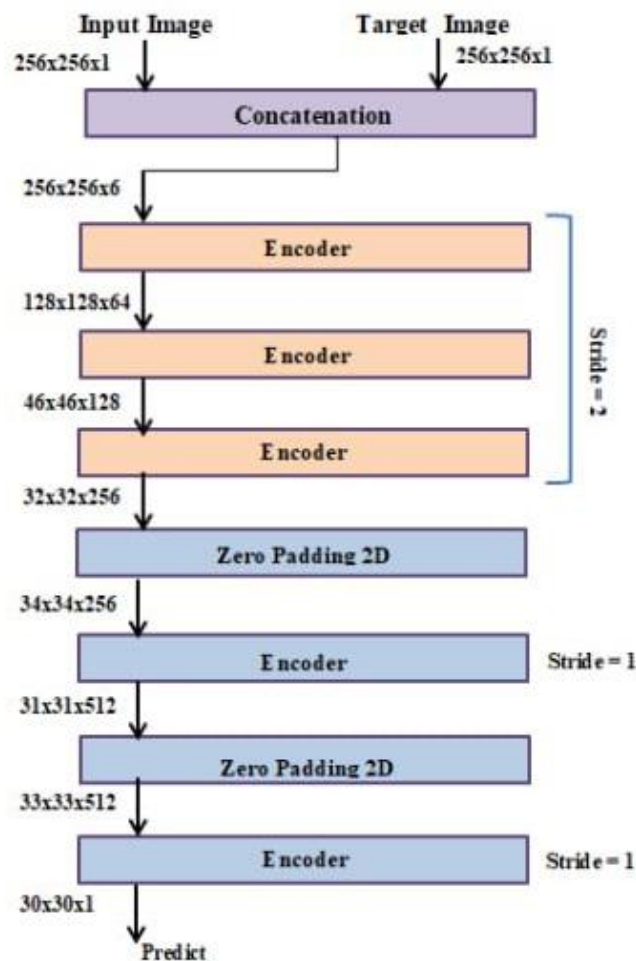


Figure 5. The structure diagram of the discriminator network utilized in our UCGAN framework

Loss Functions

One of the primary challenges encountered in training Generative Adversarial Network (GAN) models relates to establishing a suitable formulation for the loss function. The loss function is utilized to compute the distinction between the observed and expected values. Various objective functions were integrated to achieve network optimization to derive the ultimate loss function. Our UCGAN's objective function incorporates both an adversarial loss function and a pixel-wise loss function L1, which serves to penalize segmentation errors. Here, the Generator, G, is trained to minimize the objective, while the Discriminator, D, is trained to maximize the objective. Therefore, Eq. 3 can be expressed as follows.

$$G^* = \underset{G}{\operatorname{argmin}} \max_{D \in \mathcal{D}_{LCGAN}} (G, D) \quad 3$$

G transforms lung CT scans into accurate masks to minimize the cross-entropy loss of D. The adversarial loss can be interpreted as a form of structured loss, where G is penalized if the anticipated masks contain unrealistic pixels. The final objective adds the L1 loss term to Eq. 3 because the Generator aims not only to fool the Discriminator but also to minimize the pixel loss

Experimentations

Model Training and Testing

The Generator and Discriminator are concurrently optimized, with the Generator acquiring the ability to generate a plausible binary mask while the Discriminator develops the skill to distinguish between generate and authentic segmentation. Our UCGAN generator employs two methods to update its weights in the convolutional filters during training. The first method involves an internal circuit that utilizes an enhanced backpropagation technique through skip connections. The second method involves an external path, as shown in Fig. 3, which supplies the Generator with comparison results between the ground truth and the fake images generated by the Discriminator. Consequently, the Generator acquires the ability to generate segmentation maps that closely resemble the target images. Our study utilized two datasets: the training and testing sets were obtained from the COVID-19 CT Lung and Infection Segmentation Dataset³⁶. This dataset was used to train and evaluate the proposed ECGANCOVID Network, where the training set

between the real and synthetic images. The L1 loss function (Eq. 4), also known as the least absolute error, minimizes the sum of errors, and it is chosen here because it preserves sharp edges and produces less blur in the generated images⁴⁵:

$$L_{L1}(G) = E_{x,y,z} \|y - G(x, z)\|_1 \quad 4$$

Therefore, adding Eq. 4 to Eq. 3 gives the final objective used in this study in Eq. 5.

$$Loss_{UCGAN\ NET} = \underset{G}{\operatorname{argmin}} \max_{D \in \mathcal{D}_{LCGAN}} (D, G) + \lambda L_{L1}(G) \quad 5$$

The hyper parameter λ determines the magnitude of the L1 error weight⁴⁵.

This combination of loss functions, adversarial loss (for global consistency), and pixel-wise loss (for fine-grained details) can contribute to achieving the described characteristics and helps make the Model contextually aware and globally consistent. The loss functions included in our Model isolate the region of interest and its complex boundaries. Similarly, they serve as optimization techniques for extracting region, edge, and spatial features in both the encoder and decoder components of the Model.

consisted of 90% of the total images, while the testing set comprised the remaining 10%. Also, the COVID-19 CT segmentation dataset¹⁶ was utilized as an external dataset in our study to evaluate the quantification performance of our Model.

The training phase of our Model utilizes the Adam optimizer⁴⁶ as the optimizer for training weights; the objective is to minimize the segmentation loss function. The lung and lesion segmentation networks are trained with a learning rate of 2×10^{-4} , the momentum of β_1 of 0.5 and β_2 of 0.999, and a batch size of 10. The optimization process typically takes around 50 epochs to achieve convergence. Our codebase is implemented in Python, making use of the TensorFlow libraries. The experiments utilize a total of 16 gigabytes of random access memory (RAM), an Intel Core i7 processor operating at a frequency of 2.30 gigahertz, and a dedicated graphics processing unit (GPU) with 8 gigabytes of memory, specifically the NVIDIA GE-FORCE RTX model. Table 4 contains the training parameters of the UCGAN-Net utilized in the research.

Table 4. Training parameters for UCGAN-Net

Optimizer	Adam
Number of epochs	50 epochs
Loss functions	Binary cross entropy loss and L1 Loss
Momentum of β_1	0.5
Momentum of β_2	0.999
Batch size	10
Learning rate	0.0002
λ	100
patch size	70x70

Evaluation Metrics

Quantitative evaluations have been conducted to assess the proposed approach's performance in lung segmentation and infection segmentation tasks. The assessment of the segmentation tasks was done at the pixel level. In this evaluation, the positive class was defined as the foreground, which includes the lung or infected region. In contrast, the negative class was defined as the background.

Multiple major performance parameters were examined to evaluate the Model's effectiveness in effectively segmenting COVID-19 infections inside the lung. The metrics encompassed in this work consist of the dice similarity coefficient (DSC), intersection over union (IoU), Sensitivity, specificity, and Precision.

Evaluating medical image semantic segmentation, performance often involves using commonly employed metrics such as DSC and IoU. The concepts of Sensitivity and Specificity are utilized to assess the Model's capacity to differentiate between positive and negative pixels. Precision pertains to the Model's ability to make accurate predictions. The evaluation metrics are defined in the following manner:

$$\text{Intersection over Union (IoU)} = \frac{TP}{TP + FP + FN} \quad 6$$

$$\text{Dice Similarity Coefficient (DSC)} = \frac{2TP}{2TP + FP + FN} \quad 7$$

The statistical metrics IoU and DSC are utilized to evaluate the spatial overlap between binary ground truth and anticipated segmentation masks. Nevertheless, a notable distinction exists in that DSC provides a higher weight to T.P. pixels (representing accurate lung/lesion predictions) than IoU.

$$\text{Accuracy} = \frac{TP + TN}{TP + TN + FP + FN} \quad 8$$

Accuracy can be defined as the ratio of accurately classified pixels to the total number of pixels in an image.

$$\text{Precision} = \frac{TP}{TP + FP} \quad 9$$

$$\text{Sensitivity} = \frac{TP}{TP + FN} \quad 10$$

$$\text{Specificity} = \frac{TN}{TN + FP} \quad 11$$

The proportion of correctly predicted positive samples to the total number of positive class samples is called Sensitivity. Precision is a parameter that evaluates the percentage of correctly categorized positive class C.T. samples among all positive class C.T. samples. The proportion of accurately predicted negative class samples to the total number of negative class samples is referred to as specificity. The segmentation model with the highest dice similarity coefficient and IoU score is considered the best. Higher accuracy and Corona sensitivity are desirable in a classification model.

Fig. 6 illustrates the confusion matrix that may be constructed for the anticipated mask, which matches the C.T. slice. This matrix is used to calculate the aforementioned metrics based on correct predictions. P and G indicate the anticipated and ground-truth masks, respectively. In this context, TP (True Positive) indicates the count of correctly identified lung or infected pixels, TN (True Negative) signifies the count of correctly identified non-lung or uninfected pixels, FP (False Positive) corresponds to the count of infected or lung pixels erroneously identified as non-lung or non-infected pixels, and FN (False Negative) denotes the count of non-lung or uninfected pixels that are erroneously classified as lung or infected pixels.

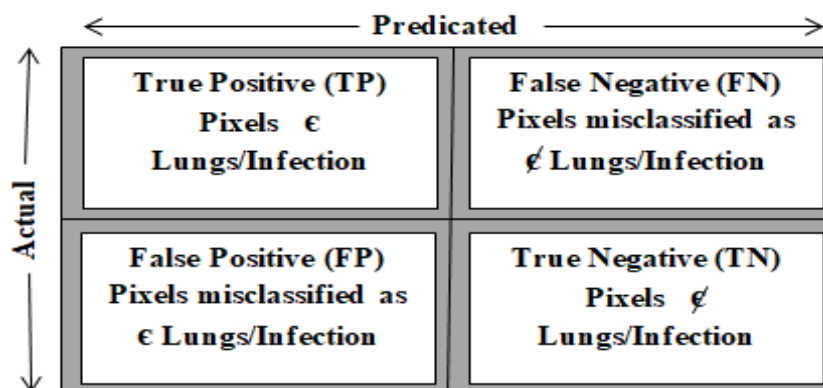


Figure 6. The confusion matrix, as well as Evaluation metrics

Results and Discussion

This section presents the quantitative results of the lung and lesion segmentation models and a comprehensive ablation study. Additionally, our Model was evaluated on a separate and independent test set. Finally, the proposed ECGANCOVID-Net's performance (that includes both UCGAN-Net1 and UCGAN-Net2) was compared with other deep models in previous studies.

Lung Segmentation

The framework under consideration, called ECGANCOVID-Net, comprises two main components: UCGAN-net1, responsible for lung segmentation, and UCGAN-net2, responsible for infection segmentation. This framework is visually depicted in Fig. 1. The purpose of these networks is to effectively and precisely delineate the boundaries between the lung and areas affected by infection in a provided C.T. picture. The main usage of the output from U-CGAN-net1 is in the post-processing phase, where it is employed to improve the performance of UCGAN-net2 and achieve precise localization of the infected region within the C.T. image. Therefore, the segmentation of the lungs plays an essential part as a pre-processing step in this process.

In this study, the UCGAN-net1 model has been applied to enhance the Precision of the cropped lung

regions in our proposed method. Table 5 presents a comprehensive overview of the quantitative outcomes obtained from the proposed Model for lung segmentation; it has been repeated in 50 epochs with batch size ten and achieved the DSC, IoU, Sensitivity, Specificity, and Precision, are 0.975, 0.9538, 0.9750, 0.9983, and 0.9766, respectively which is demonstrated in it.

Table 5. The quantitative outcomes of the UCGAN Net1 model on the test set derived from the COVID-19 CT Lung and Infection Segmentation Dataset.

DSC(%)	IOU(%)	SENS. (%)	Speci.(%)	Pre.(%)
97.5	95.4	97.5	99.8	97.7

Table 6 demonstrates that our lung segmentation network can enhance the original segmentation performance of the Dice Similarity Coefficient by 3.6%. Additionally, compared to other state-of-the-art segmentation models, it achieves improvements of 6.4%, 1.0%, and 8.3% in terms of Intersection over Union (IOU), Specificity, and Precision.

Table 6. Comparison of the lung segmentation outcomes achieved by employing the most advanced deep-learning models and the proposed UCGAN Net1. (The most optimal outcomes are presented in bold formatting.)

Architecture	DSC(%)	IOU(%)	SENS. (%)	Speci.(%)	Pre.(%)
UNET	53.9	42.1	80.8	74.3	42.3
ATTEN RES UNET	93.6	88.5	99.5	98.8	88.7
ATTEN UNET	93.9	89.0	99.3	98.8	89.4
UCGAN NET1(ours)	97.5	95.4	97.5	99.8	97.7

Despite the significant impact of COVID-19 on the lungs, the trained Model successfully achieved accurate segmentation of the lung boundaries, as

demonstrated in Fig. 7. This outcome underscores the strong performance and reliability of this study's proposed lung segmentation model.

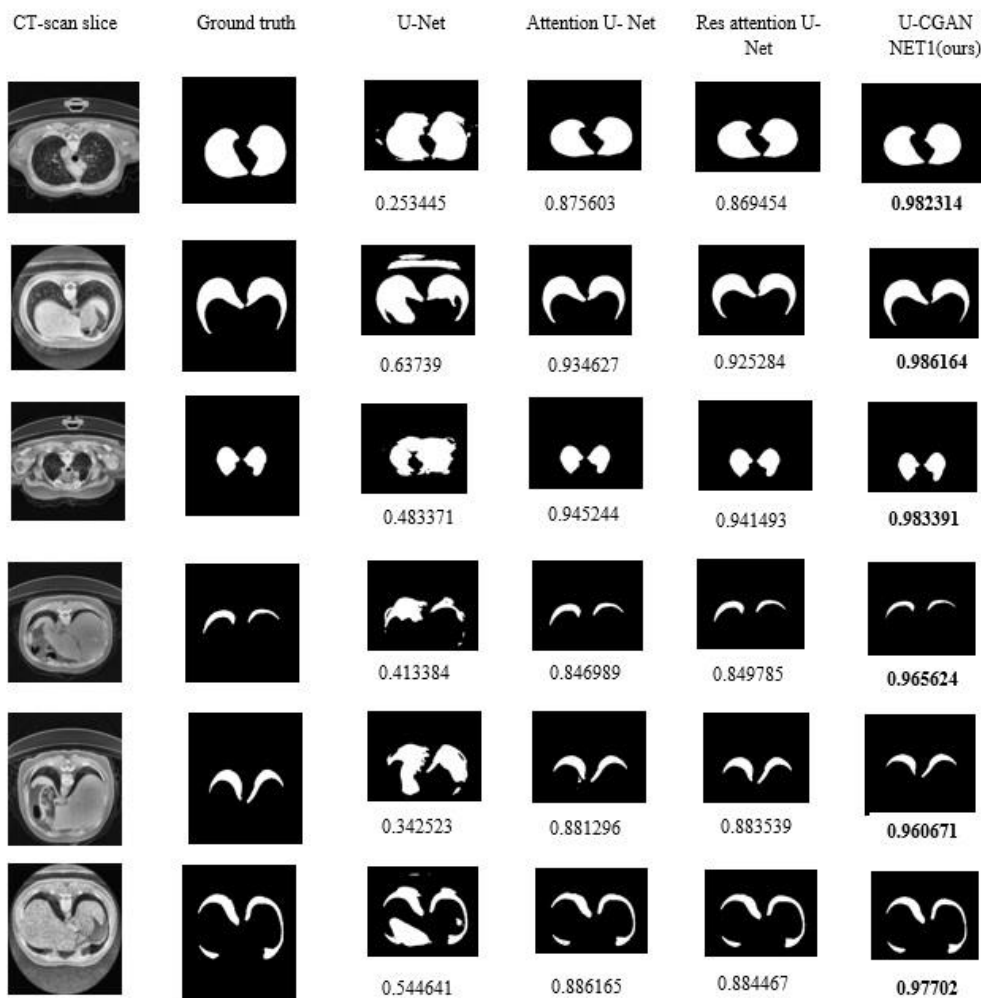


Figure 7. The first row of the shown images consists of C.T. images, while the second row represents the ground truth. The subsequent rows (3-6) display the segmentation masks generated by three networks and our network. Additionally, the dice score values for each segmentation mask are provided

COVID-19 Lesion Segmentation:

To illustrate the impact of each component on the performance of the proposed Model, an ablation study was conducted. Initially, the Model was trained without integrating the first UCGAN1 NET into the architecture of ECGANCOVID-NET. Subsequently, UCGAN1 NET was integrated into our Model but excluded the use of the Horizontal flipping data augmentation technique. Finally, the performance of the proposed Model trained with data augmentation has been examined.

Table 7 presents the results of different configurations of the examined models. The baseline model yielded DSC and IoU scores of 76.0% and

65.5%, respectively. This initial assessment suggests the potential for improving model performance through the implementation of a hierarchical segmentation strategy using cascaded UCGAN-Nets models. Rather than directly segmenting the COVID-19-infected area, our approach generates lung contour maps from the predicted lung mask. These contour maps are subsequently utilized as input for another UCGAN-Net model to accurately localize the infected regions. In the case of infection segmentation by hierarchical segmentation (ECGANCOVID), the DSC improves by 7.3% compared to the direct segmentation model.

Expanding our dataset and training our Model on it achieved gains of 8.5% and 13% in DSC and IoU scores, respectively, when compared to the baseline

model. This demonstrates the positive impact of dataset expansion and training on enhancing the Model's segmentation performance.

Table 7. Ablation study on our model test results

Models used	DSC%	IOU%	SENS. %	Pre. %
Direct segmentation (U-CGAN Net)	76.0	65.5	73.8	81.7
Hierarchal segmentation(ECGANCOVID Net) Without data augmentation	83.3	73.6	79.8	89.7
Hierarchal segmentation(ECGANCOVID Net) With data Augmentation	84.5	78.5	84.6	85.8

The DSC of 84.5 and IOU of 78.5 for COVID-19 lesion segmentation demonstrate a significant level of Precision in our Model's capacity to detect and delineate lesions. Within a clinical context, these metrics are essential as they indicate the Model's efficacy in accurately detecting and delineating the actual extent of lesions in relation to the ground truth. A greater DSC and IOU indicate a stronger correspondence between the Model's predictions and the real lesions. The clinical utility of such performance is significant where Healthcare professionals rely on accurate segmentation for various purposes, including disease diagnosis, treatment planning, and monitoring disease progression.

Among the several evaluation metrics, it is observed that the Precision metric yields a value of 85.8, signifying that the Model produces around 14% erroneous positive predictions when applied to the test set. Additionally, it is noteworthy that the metric sensitivity value of the ECGANCOVID model is considerably greater than other measures. This suggests that the Model performs better in accurately identifying and localizing the intricate patterns associated with the infection.

The exceptional performance across DSC, IOU, Precision, and Sensitivity metrics enhances the clinical utility of the Model. It suggests that the Model is accurate, reliable, and effective in lesion segmentation, providing valuable information for clinicians to diagnose and treat COVID-19 cases.

Table 8. A comparative analysis evaluates the test results of both state-of-the-art and proposed models. The test set utilized in this analysis is obtained from the COVID-19 CT Lung and Infection Segmentation Dataset³⁶.

Architecture	DSC(%)	IOU(%)	SENS. (%)	Pre.(%)
ATTEN RES UNET	77.8	65.9	78.0	81.1
ATTENTION UNET	74.8	63.1	72.9	80.5
ECGANCOVID Net(ours)	83.3	73.6	79.8	89.7

Furthermore, the obtained results are compared to various advanced segmentation models, as shown in Table 8. The ECGANCOVID-Net approach outperformed other techniques, significantly enhancing evaluation metric values. The Dice Similarity Coefficient (DSC) and Intersection over Union (IOU) scores quantify the degree of overlap between the predicted lesions and the actual ground truth. Higher scores of our Model indicate precise delineation of lesions, providing crucial information for diagnosis and treatment planning. Our Model's Precision, at 89.7%, underscores its ability to reliably identify positive cases (lesions) and reduce the occurrence of false positives in clinical scenarios compared with other baseline models. The increased

Precision of the Model enhances its reliability in generating accurate predictions, which is crucial for clinical decision-making.

ECGANCOVID Model's high Sensitivity augments its utility in detecting lesions, which is particularly important for early detection and appropriate treatment of COVID-19-related lesions. These measures collectively affirm that the ECGANCOVID Model is clinically valuable and successful in accurately segmenting lesions.

Fig. 8 shows the segmentation networks' prediction samples. The results collected demonstrate our Net's better performance than other networks. The ATTENTION UNET and Direct segmentation (UCGAN Net) have shown the ability

to segment large lesions accurately. Nonetheless, the performance of both models on tiny lesions is mediocre. On the other hand, the ECGANCOVID-NET outperformed in accurately identifying small lesions in the cases presented in Fig. 8 (second, fourth, fifth, and seventh).

Furthermore, the segmentation performance of ATTENTION RESIUAL UNet is better than theirs, but the error rates of these three models on boundaries are still very high. Compared with these three typical models, the overall performance of our Model on small lesions is better.

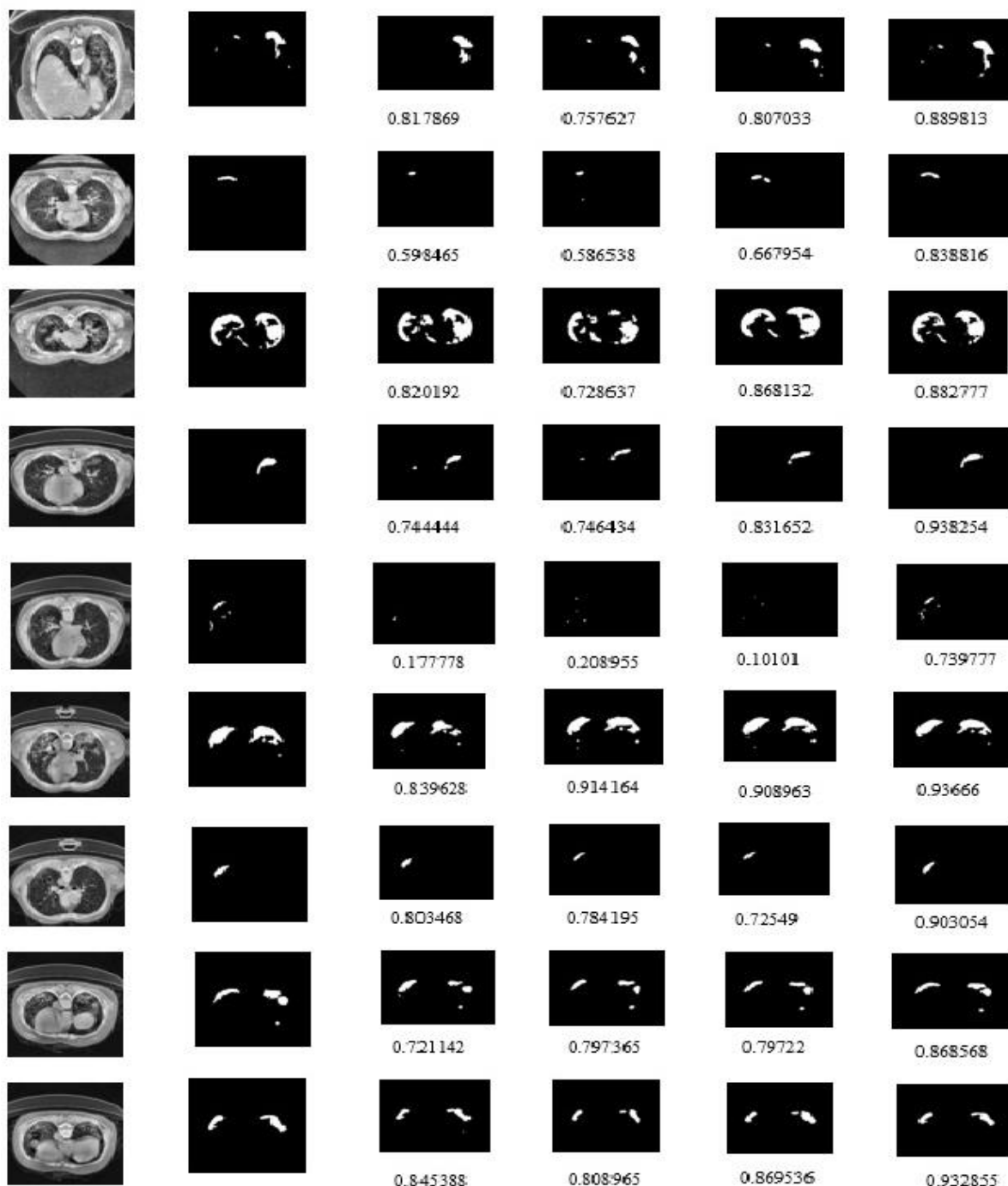


Figure 8. displays the prediction outcomes of various representative models. In this study, the C.T. image was denoted as A, the ground truth as B, the results of Attention UNet as C, the results of Attention Residual UNet as D, the results of direct segmentation using UCGAN Net as E, and the results of hierarchical segmentation using ECGANCOVID Net as F.

Assessment of the ECGANCOVID Model's Generalization :

After training the two UCGAN networks and integrating the entire analysis pipeline into the ECGANCOVID system, a separate set of unseen data that was not used during training was utilized to assess the generalization capabilities of the Model, specifically the COVID-19 CT segmentation dataset³⁷. External validation with an unseen dataset is a crucial step to verify the reliability and effectiveness of ECGANCOVID-Net in real-world applications beyond the training data. The main objective is to assess how well the Model generalizes its learned patterns to new, unseen instances, gauging its ability to handle data previously exposed.

The performance metrics for the entire process were quantified using measures such as DSC, IOU,

Precision, and Accuracy (refer to Table 9). During our observation, a perfect overlap was noted between the predicted and reference lesion masks regarding the Dice Similarity Coefficient (DSC) and Intersection over Union (IOU) achieved by our Model. The metrics for infection segmentation show an improvement of 14.9% and 15.0%, respectively. However, it is worth noting that the precision metric has the lowest value, indicating that the ECGANCOVID model generates approximately 37% of false positive predictions from the external test dataset compared to other baseline segmentation models. Fig. 9 visually compares the lung and lesion masks generated by the ECGANCOVID Net and the reference masks.

Table 9. Comparison of test results obtained from two of the most effective baseline segmentation techniques and our proposed approach in the context of COVID-19 lesion segmentation on an external dataset³⁷.

Architecture	DSC(%)	IOU(%)	Prec(%)	ACCU.(%)
ATTEN UNET	45.3	32.5	38.2	97.5
ATTEN RES UNET	54.8	41.8	46.4	98.0
ECGANCOVID NET(our)	69.7	56.8	62.6	99.2

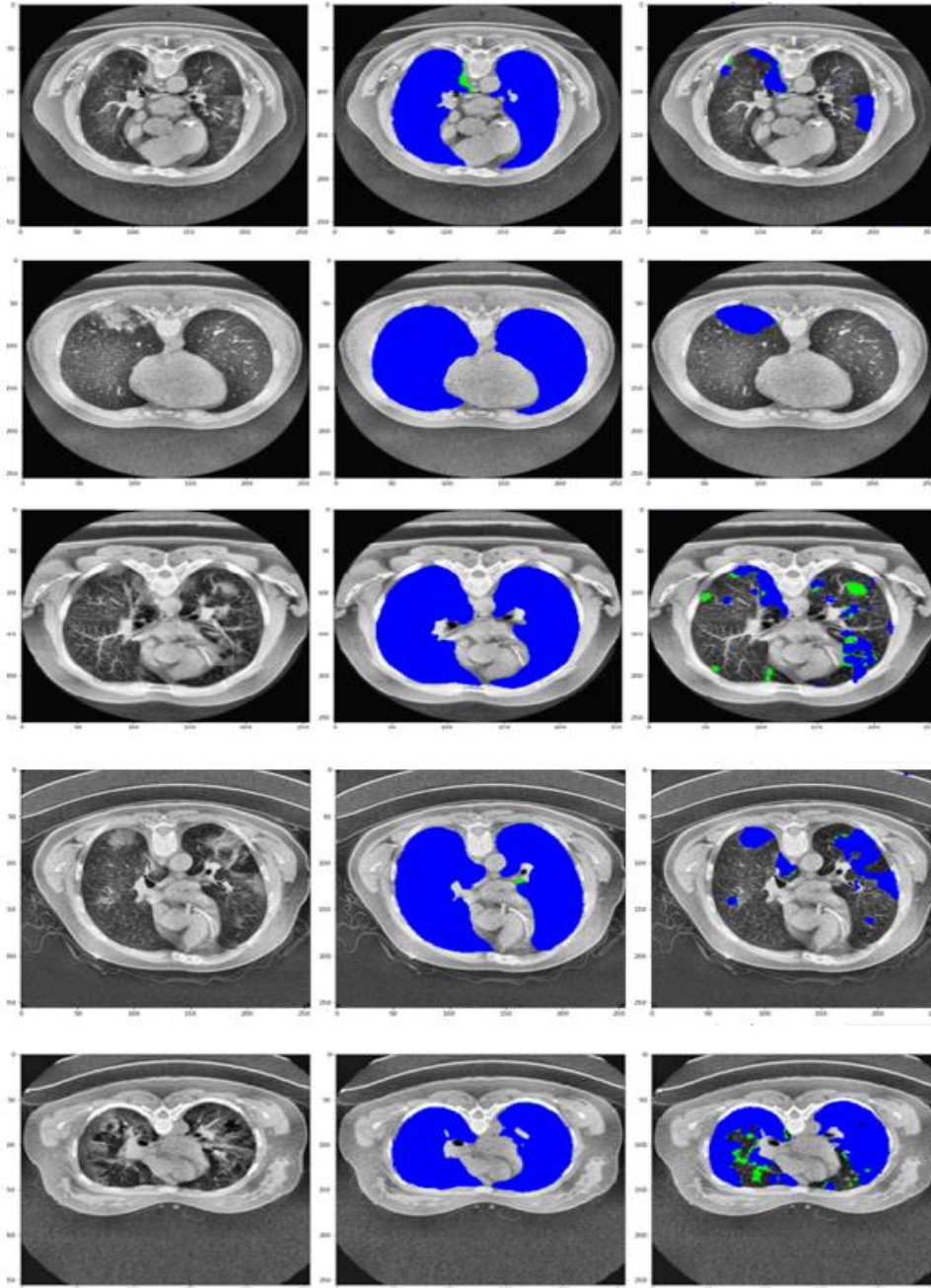


Figure 9. The rows display five samples (patient 1, patient 3, patient 4, patient 5, and patient 9) obtained from the COVID-19 CT segmentation³⁷ test dataset. The columns consist of the following: the original images are displayed on the left side. At the same time, the overlays between the predicted lung masks and the reference lung masks are shown in the center column. Lastly, the overlays between the predicted COVID-19 lesion masks and the reference COVID-19 lesion masks are displayed in the right column. The reference masks are shown in green, while the anticipated masks generated by the ECGANCOVID system are represented in blue.

Comparison of ECGANCOVID Model with Prior Works:

To perform a comprehensive assessment, our results were compared with those obtained by other researchers using the same publicly available dataset. The relevant work was organized and condensed in Tables 10 and 11. Our model outperforms all other models with a DSC of 84.5%, Precision of 85.8%, and Specificity of 99.9%. The authors in ⁴⁷ developed a novel neural network architecture, CHS-Net (COVID-19 hierarchical segmentation network), specifically designed for COVID-19 infection segmentation. CHS-Net and ECGANCOVID-NET were trained on 2D CT scans and achieved COVID-19 infection segmentation DSCs of 0.816 and 0.845, respectively. It is important to mention that CHS-Net is based on a UNet with two cascaded residual attention inception UNet networks in a sequence of encoder-decoders for Corona infection segmentation. Our model was able to outperform the CHS-Net network and addressed the problem presence of false positives in the results produced by it, which generated approximately 25% of false positive predictions using hybrid loss functions in ECGANCOVID, where our model successfully reduced number of false positive predictions by 11%.

Based on the Ma et al. dataset³⁶, ECGANCOVID achieved a specificity of 99.9%, outperforms other architectures for COVID-19 infection; this indicates our Model's effectiveness in capturing and correctly delineating the target region in comparison to the total actual pixels in that region. The findings presented in Table 11 indicate that utilizing our lesion segmentation model on CT images can substantially enhance the Model's performance where our Model can accurately identify and segment 84.6% of the actual positive lesions out of the total lesions present in the test dataset. It outperformed all other approaches mentioned in

Table 11 and achieved results close to those in references ^{48,49}. Given the advances in the proposed method, The following highlights are to be emphasized:

- The ECGANCOVID Net architecture exhibits good results for segmenting lung parenchyma and areas affected by COVID-19, compared with the results obtained by related works that employed the same public dataset.
- The proposed method successfully segments areas affected by COVID-19, particularly in accurately identifying tiny lung lesions from its hierarchical segmentation strategy executed via the proposed cascaded UCGAN Nets with 70x70 PatchGAN architecture. This is extremely useful, providing specialists with new perspectives for analyzing the lesion.
- The proposed approach involves training the loss function by taking into account the full image rather than focusing on pixel-wise loss. This method enhances their contextual awareness and promotes global consistency. Including L1 loss helps to preserve fine details in the generated images and Adversarial training contributes to capturing global structures and improving the overall visual quality of the generated images.
- To avoid overfitting and dealing with required paired data for training, data augmentation strategies like rotation are used. Model learning had been successfully enhanced by 1.50% and 2.90% in the Dice Similarity Coefficient for lung and lesion segmentation, respectively.

While the ECGANCOVID model provided better results, the question of how to reduce the presence of false positive predictions in the results produced by our architecture remains an important consideration.

Table 10. Comparison of our proposed UCGAN Net1 with other deep models in previous studies on lung segmentation

References	Year	Model (Method)	DCS%
2	2020	3D UNet and Residual Unet	95.6
50	2021	3D Unet	95.6
51	2022	two cascaded deep FCNs	96.1
47	2022	CHS-Net	96.3
52	2023	DLShelper	96.0
Ours		UCGAN net1	97.5

Table 11. Comparison of the proposed ECGANCOVID model with other deep models in previous studies On COVID-19 infection Segmentation

References	Year	Model (Method)	DCS	Sen.	Prec.	Spec.
53	2020	CoSinGAN	61.5	-	-	-
33	2020	Semi-Inf-Net	73.9	72.5	-	96.0
54	2020	MultiResUNet	74.3	-	-	-
2	2020	3D UNet and Residual UNet	76.1	73.0	-	99.9
38	2021	3D UNet	67.3	-	-	-
55	2021	3D UNet	70.4	68.2	-	-
56	2021	D2A UNet	72.98	-	-	-
57	2021	LCFCN	75.0	86	-	97
50	2021	3D UNet	80.4	-	-	-
48	2021	MiniSeg segmentation network	76.3	85.06	-	99
49	2021	3D CU-Net	77.1	83.7	-	99.8
58	2021	PSGR UNet, PSGR U2Net	78.6	77.83	-	99.8
59	2021	LungINFseg	80.3	83.1	-	99.5
47	2022	CHS-Net	81.6	-	75.6	96.9
60	2022	HADCNet	72.3	69.4	-	99.7
61	2022	SSA-Net	65.2	-	-	-
62	2022	D MDF-Net	75.7	72.78	-	99.8
51	2022	two cascaded deep FCNs	78.0	82.2	-	95.1
63	2023	U2 -Net+PSGR module	78.6	77.83	-	99.8
64	2023	SELDNet	79.1	76.3	-	96.7
65	2023	Cov-TransNet	80.3	77.2	84.2	99.5
Ours		ECGANCOVID	84.5	84.6	85.8	99.9

Limitation:

Obtaining extensive data for effective training is crucial to ensure the Model's robustness. One of the limitations of this study is the scarcity of publicly available annotated imaging datasets which have diverse imaging data, including various COVID-19 states, other pneumonia cases, healthy control samples, and comprehensive clinical and laboratory information). This makes the current segmentation approach in our research biased due to it is only trained with COVID-19-related images for lung lesion segmentation that is used as the first step of

severity assessment and prediction of COVID-19 patients since COVID-19 has close similarities with viral pneumonia diseases like influenza, and other pneumonia, or entirely unrelated medical conditions like cancer, eliciting distinct features for diagnosed task a great challenge. So the patients with COVID-19 needed to be diagnosed with various features along with Chest CT scan images such as clinical and laboratory features. To guarantee the robustness and comparability of models, building comprehensive, accepted public benchmark datasets is essential.

Conclusion

One of the biggest problems in the localization of lesion areas task is the identification of boundaries that arise due to the image resolution, where The organ's tissues appearing in the CT scan may lead to mixing the categories of pixels. To tackle this problem, an approach called ECGANCOVID-Net, a hierarchical segmentation network that detects regions affected by COVID-19 in lung contour maps

obtained from computed tomography (C.T.) images, has been proposed. The proposed method consists of two cascaded UCGAN Net models that employ the adversarial terms in training, and it foists higher-order spatial consistency instead of spatial contiguity. The UCGAN model enhances the performance of a conditional generative adversarial network by incorporating advanced components to

modify its Generator and Discriminator. Our Model was trained successfully on chest C.T. photos and corresponding ground truth masks for lung and lesion, obtained from a publicly available dataset known as the COVID-19 CT Lung and Infection Segmentation Dataset.

To demonstrate the effectiveness of our methodology, an ablation analysis was performed to assess the Model's performance. Furthermore, a comparative analysis of the performance of our proposed methodology with several popular baseline architectures utilized for COVID-19 segmentation, including Unet, attention Unet, and Atten res Unet, has been conducted. Additionally, our results were compared with those obtained by other researchers who employed the same publicly available dataset. The experimental findings showed that the suggested Model has improved performance in segmenting areas affected by COVID-19, particularly in accurately identifying tiny lung lesions.

The ECGANCOVID-Net model, after implementing data augmentation techniques, has demonstrated notable performance in various evaluation metrics and higher localization performance with 84.5% DSC, while the IOU (Intersection over Union) score achieved 78.5%. Additionally, the precision score obtained a value of 85.8%, indicating that the Model generated approximately 14% false positive predictions from the test set. Moreover, the Model exhibited a

COVID-19 sensitivity of 84.6%, surpassing the performance of other existing models.

The suggested methodology can potentially be a valuable tool for healthcare professionals in managing COVID-19 because it offers the opportunity for quantitative assessment and disease monitoring as applications in clinical studies where our Model is used as the first step of severity assessment and prognosis prediction of COVID-19 patients. Therefore, our system could facilitate early intervention and provide a unified solution that helps physicians assess the severity and track the progression of the illness.

In the future, this study could be expanded in several aspects. To enhance the portability and robustness of the model, training and testing could be conducted using a larger dataset. Hierarchical data augmentation techniques could be employed to address the challenges posed by small datasets, and modifications to the architecture of ECOVIDCGAN could be implemented. For instance, changes to loss functions and the CNN-based Generator and Discriminator could design a comprehensive system for automatic localization, segmentation, and analysis of COVID-19 pneumonia lesions. Furthermore, extending ECOVIDCGAN lesion segmentation into a hybrid deep-learning model for infection quantification and detecting high-risk COVID-19 patients based on CT images and clinical and laboratory features could be explored.

Authors' Declaration

- Conflicts of Interest: None.
- We hereby confirm that all the Figures and Tables in the manuscript are ours. Furthermore, any Figures and images, that are not ours, have been included with the necessary permission for re-publication, which is attached to the manuscript.
- No animal studies are present in the manuscript.
- No human studies are present in the manuscript.
- Ethical Clearance: The project was approved by the local ethical committee at University of write the name of the university or center of which you received the approval.

Authors' Contributions Statement

This work was carried out in collaboration between all authors. P.H.H. and I.H.A. participated in configuring the idea of the paper and solving the problem statement. P.H.H. participated in the

training model, interpreted the results, and Wrote the paper. The researcher, I.H.A., interpreted the results and reviewed and proofread the paper.

References

1. Kakodkar P, Kaka N, Baig M. A Comprehensive Literature Review on the Clinical Presentation and Management of the Pandemic Coronavirus Disease 2019 (COVID-19). *Cureus*. 2020; 18. <https://doi.org/10.7759/cureus.7560>

2. Muller D, Soto-rey I, Kramer F. Automated Chest CT Image Segmentation of COVID-19 Lung Infection based on 3D U-Net. arXiv preprint arXiv:2007.04774.2020.
3. Mansoor A, Bagci U, Foster B, Xu Z, Papadakis GZ, Folio LR, et al. Segmentation and image analysis of abnormal lungs at CT: Current approaches, challenges, and future trends. *Radiographics*. 2015; 35(4): 1056–1076. <https://doi.org/10.1148%2Frg.2015140232>
4. Kass M, Witkin A, Terzopoulos D. Snakes: Active contour models. *Int J Comput Vis*. 1988; 1(4): 321–31. <https://doi.org/10.1007/BF00133570>
5. Malladi R, Sethian JA, Vemuri BC. Shape Modeling with Front Propagation: A Level Set Approach. *IEEE Trans Pattern Anal Mach Intell*. 1995; 17(2): 158–175. <https://doi.org/10.1109/34.368173>
6. Beucher S, Lantuejoul C. Use of Watersheds in Contour Detection. *International Workshop on Image Processing: Real-time Edge and Motion Detection/Estimation*. 1979;(January 1979): 12–21.
7. Adams R, Bischof L. Seeded Region Growing. *IEEE Trans Pattern Anal Mach Intell*. 1994; 16(6): 641–7. <https://doi.org/10.1109/34.295913>
8. Manjunath BS, Chellappa R. Unsupervised Texture Segmentation Using Markov Random Field Models. *IEEE Trans Pattern Anal Mach Intell*. 1991; 13: 478–482. <https://doi.org/10.1109/34.134046>
9. Han C, Duan Y, Tao X, Lu J. Dense Convolutional Networks for Semantic Segmentation. *IEEE Access*. 2019; 7: 43369–82. <https://doi.org/10.1109/ACCESS.2019.2908685>
10. Weng W, Zhu X. INet: Convolutional Networks for Biomedical Image Segmentation. *IEEE Access*. 2021; 9: 16591–603. <https://doi.org/10.1109/ACCESS.2021.3053408>
11. Oktay O, Schlemper J, Folgoc L Le, Lee M, Heinrich M, Misawa K, et al. Attention U-Net: Learning Where to Look for the Pancreas. arXiv preprint arXiv:1804.03999. 2018; <https://doi.org/10.48550/arXiv.1804.03999>
12. Md Zahangir Alom, Chris Yakopcic, Tarek M Taha, Vijayan K. Recurrent Residual Convolutional Neural Network based on U-Net (R2U-Net) for Medical Image Segmentation. arXiv preprint arXiv:1802.06955. 2018; <https://doi.org/10.48550/arXiv.1802.06955>
13. Goodfellow I, Pouget-Abadie J, Mirza M, Xu B, Warde-Farley D, Ozair S, et al. Generative adversarial networks. *Commun ACM*. 2020; 63(11): 7. <https://doi.org/10.1145/3422622>
14. Mirza M, Osindero S. Conditional Generative Adversarial Nets. arXiv preprint arXiv:1411.1784. 2014. <https://doi.org/10.48550/arXiv.1411.1784>
15. Salman AO, Geman O. Evaluating Three Machine Learning Classification Methods for Effective COVID-19 Diagnosis. *Int J Math Comput Sci*. 2023 Jan 15; 1: 1–14. <http://dx.doi.org/10.59543/ijmscs.v1i.7693>
16. Arif ZH, Cengiz K. Severity Classification for COVID-19 Infections based on Lasso-Logistic Regression Model. *Int J Math Comput Sci*. 2023; 1: 25–32. <https://dx.doi.org/10.59543/ijmscs.v1i.7715>
17. Abdulkareem KH, Al-Mhiqani MN, Dinar AM, Mohammed MA, Al-Imari MJ, Al-Waisy AS, et al. MEF: Multidimensional Examination Framework for Prioritization of COVID-19 Severe Patients and Promote Precision Medicine Based on Hybrid Multi-Criteria Decision-Making Approaches. *Bioengineering*. 2022; 9(9): 457–489. <https://doi.org/10.3390/bioengineering9090457>
18. Li Y, Wei D, Chen J, Cao S, Zhou H, Zhu Y, et al. Efficient and Effective Training of COVID-19 Classification Networks with Self-Supervised Dual-Track Learning to Rank. *IEEE J Biomed Health Inform*. 2020 ;24(10): 2787–2797. <https://doi.org/10.1109/JBHI.2020.3018181>
19. Owais M, Baek NR, Park KR. Domain-adaptive artificial intelligence-based model for personalized diagnosis of trivial lesions related to COVID-19 in chest computed tomography scans. *J Pers Med*. 2021 Oct 1; 11(10). <https://doi.org/10.3390/jpm11101008>
20. Mondal MRH, Bharati S, Podder P. CO-IRv2: Optimized InceptionResNetV2 for COVID-19 detection from chest CT images. *PLoS One*. 2021; 16(10 October): 1–24. <https://doi.org/10.1371/journal.pone.0259179>
21. Hasan N, Bao Y, Shawon A, Huang Y. DenseNet Convolutional Neural Networks Application for Predicting COVID-19 Using CT Image. *SN Comput Sci*. 2021; 2(5): 1–11. <https://doi.org/10.1007/s42979-021-00782-7>
22. Zhang X, Lu S, Wang SH, Yu X, Wang SJ, Yao L, et al. Diagnosis of COVID-19 Pneumonia via a Novel Deep Learning Architecture. *J Comput Sci Technol*. 2022; 37(2): 330–43. <https://doi.org/10.1007/s11390-020-0679-8>
23. Motwani A, Shukla PK, Pawar M, Kumar M, Ghosh U, Numay W Al, et al. Enhanced Framework for COVID-19 Prediction with Computed Tomography Scan Images using Dense Convolutional Neural Network and Novel Loss Function. *Comput Electr Eng*. 2022; 105: 108479. <https://doi.org/10.1016/j.compeleceng.2022.108479>
24. Podder P, Das SR, Mondal MRH, Bharati S, Maliha A, Hasan MJ, et al. LDDNet: A Deep Learning Framework for the Diagnosis of Infectious Lung Diseases. *Sensors*. 2023; 23(1). <https://doi.org/10.3390/s23010480>
25. Minaee S, Kafieh R, Sonka M, Yazdani S, Jamalipour Soufi G. Deep-COVID: Predicting COVID-19 from chest X-ray images using deep transfer learning. *Med Image Anal*. 2020 Oct 1; 65. <https://doi.org/10.1016/j.media.2020.101794>
26. Mohammed MA, Al-Khateeb B, Yousif M, Mostafa SA, Kadry S, Abdulkareem KH, et al. Novel Crow Swarm Optimization Algorithm and Selection

- Approach for Optimal Deep Learning COVID-19 Diagnostic Model. *Comput Intell Neurosci*. 2022; 2022. <https://doi.org/10.1155/2022/1307944>
27. Long, Jonathan, Evan Shelhamer, and Trevor Darrell. Fully convolutional networks for semantic segmentation. *Proc IEEE Conf Comput Vis Patt Rec*. 2015; 3431-3440. <https://doi.org/10.48550/arXiv.1411.4038>
28. Ouyang X, Huo J, Xia L, Shan F, Liu J, Mo Z, et al. Dual-Sampling Attention Network for Diagnosis of COVID-19 from Community Acquired Pneumonia. *IEEE Trans Med Imaging*. 2020; 39(8): 2595-2605 <https://doi.org/10.48550/arXiv.2005.02690>
29. Amyar A, Modzelewski R, Li H, Ruan S. Multi-task deep learning based CT imaging analysis for COVID-19 pneumonia: Classification and segmentation. *Comput Biol Med*. 2020; 126. <https://doi.org/10.1016/j.combiomed.2020.104037>
30. Yan Q, Wang B, Gong D, Luo C, Zhao W, Shen J, et al. COVID-19 Chest CT Image Segmentation --A Deep Convolutional Neural Network Solution. *arXiv preprint arXiv:2004.10987*. 2020 ; <https://doi.org/10.48550/arXiv.2004.10987>
31. Hu S, Gao Y, Niu Z, Jiang Y, Li L, Xiao X, et al. Weakly Supervised Deep Learning for COVID-19 Infection Detection and Classification from CT Images. *IEEE Access*. 2020; 8: 118869–118883 . <https://doi.org/10.48550/arXiv.2004.06689>
32. Oulefki A, Agaian S, Trongtirakul T, Kassah Laouar A. Automatic COVID-19 lung infected region segmentation and measurement using CT-scans images. *Pattern Recognit*. 2021 Jun 1; 114. <https://doi.org/10.1016/j.patcog.2020.107747>
33. Fan DP, Zhou T, Ji GP, Zhou Y, Chen G, Fu H, et al. Inf-Net: Automatic COVID-19 Lung Infection Segmentation from CT Images. *IEEE Trans Med Imaging*. 2020 Apr 22; 39(8): 2626-2637. <https://doi.org/10.1109/tmi.2020.2996645>
34. Mu N, Wang H, Zhang Y, Jiang J, Tang J. Progressive global perception and local polishing network for lung infection segmentation of COVID-19 CT images. *Pattern Recognit*. 2021 Dec 1; 120. <https://doi.org/10.1016/j.patcog.2021.108168>
35. He J, Zhu Q, Zhang K, Yu P, Tang J. An evolvable adversarial network with gradient penalty for COVID-19 infection segmentation. *Appl Soft Comput*. 2021 Dec 1; 113. <https://doi.org/10.1016/j.asoc.2021.107947>
36. COVID-19 CT Lung and Infection Segmentation Dataset | Zenodo . 2020.
37. COVID-19 - Medical segmentation. 2020.
38. Ma J, Wang Y, An X, Ge C, Yu Z, Chen J, et al. Toward data-efficient learning: A benchmark for COVID-19 CT lung and infection segmentation. *Med Phys*. 2020; 48(3): 1197–210. <https://doi.org/10.1002/mp.14676>
39. Radiopaedia.org, the peer-reviewed collaborative radiology resource.. <https://radiopaedia.org/>
40. Coronacases.org – by Raioss.com [Internet]. [cited 2023 Jul 23] .
41. Pizer SM, Philip Amburn E, Austin JD, Cromartie R, Geselowitz A, Greer T, et al. Adaptive Histogram Equalization and Its Variations. *Comput Vis Graph Image Process*. 1987; 39(3): 355-368 . [https://doi.org/10.1016/S0734-189X\(87\)80186-X](https://doi.org/10.1016/S0734-189X(87)80186-X)
42. Zimmerman JB, Pizer SM, Staab E V, Perry JR, McCartney W, Brenton BC. An Evaluation of the Effectiveness of Adaptive Histogram Equalization for Contrast Enhancement. *IEEE Trans Med Imaging*. 1988; 7(4): 304-312. <https://doi.org/10.1109/42.14513>
43. Pizer SM, Johnston RE, Ericksen JP, Yankaskas BC, Muller KE. Contrast-Limited Adaptive Histogram Equalization: Speed and Effectiveness. *Proceedings of the first conf. on visual. in biomedical computing*.1990. <https://doi.org/10.1109/VBC.1990.109340>
44. Khalifa NE, Loey M, Mirjalili S. A comprehensive survey of recent trends in deep learning for digital images augmentation. *Artif Intell Rev* . 2022; 55(3): 2351–77. <https://doi.org/10.1007/s10462-021-10066-4>
45. Isola P, Zhu JY, Zhou T, Efros AA. Image-to-image translation with conditional adversarial networks. *Proc. - 30th IEEE Conf Comput Vis Patt Rec*. 2017; 1125-1134. <https://doi.org/10.48550/arXiv.1611.07004>
46. Ruder S. An overview of gradient descent optimization algorithms. *arXiv preprint arXiv: 1609.04747*. 2016 ; <https://doi.org/10.48550/arXiv.1609.04747>
47. Punn NS, Agarwal S. CHS-Net: A Deep Learning Approach for Hierarchical Segmentation of COVID-19 via CT Images. *Neural Process Lett*. 2022; 54(5): 3771–92. <https://doi.org/10.1007/s11063-022-10785-x>
48. Qiu Y, Liu Y, Li S, Xu J. MiniSeg: An Extremely Minimum Network for Efficient COVID-19 Segmentation. *35th AAAI Conference on Artificial Intelligence, AAAI 2021*. 2021; 6A: 4846–54. <https://doi.org/10.48550/arXiv.2004.09750>
49. Zheng R, Zheng Y, Dong-Ye C. Improved 3D U-Net for COVID-19 Chest CT Image Segmentation. *Sci Program*. 2021; 2021. <https://doi.org/10.1155/2021/9999368>
50. Müller D, Soto-Rey I, Kramer F. Robust chest CT image segmentation of COVID-19 lung infection based on limited data. *Inform Med Unlocked*. 2021; 25: 11 <https://doi.org/10.1016/j.imu.2021.100681>
51. Alirr OI. Automatic deep learning system for COVID-19 infection quantification in chest CT. *Multimed Tools Appl* . 2022; 81(1): 527–41. <https://doi.org/10.1007/s11042-021-11299-9>
52. He T, Liu H, Zhang Z, Li C, Zhou Y. Research on the Application of Artificial Intelligence in Public Health Management: Leveraging Artificial Intelligence to Improve COVID-19 CT Image Diagnosis. *Int J*

- Environ Res Public Health. 2023; 20(2): 1158-1170.
<https://doi.org/10.3390/ijerph20021158>
53. Zhang P, Zhong Y, Deng Y, Tang X, Li X. CoSinGAN: Learning COVID-19 infection segmentation from a single radiological image. *Diagnostics*. 2020;10(11):1–28.
<https://doi.org/10.3390/diagnostics10110901>
54. Yang Q, Li Y, Zhang M, Wang T, Yan F, Xie C. Automatic Segmentation of COVID-19 CT Images using improved MultiResUNet. *Proc 2020 Chinese Autom Congr.* 2020; 1614-1618..
<https://doi.org/10.1109/CAC51589.2020.9327668>
55. Wang Y, Zhang Y, Liu Y, Tian J, Zhong C, Shi Z, et al. Does non-COVID-19 lung lesion help? investigating transferability in COVID-19 CT image segmentation. *Comput Methods Programs Biomed* . 2021; 202: 106004.
<https://doi.org/10.1016/j.cmpb.2021.106004>
56. Zhao X, Zhang P, Song F, Fan G, Sun Y, Wang Y, et al. D2A U-Net: Automatic Segmentation of COVID-19 Lesions from CT Slices with Dilated Convolution and Dual Attention Mechanism. *arXiv preprint arXiv:2102.05210*. 2021; 11 .
<https://doi.org/10.1016/j.compbimed.2021.104526>
57. Laradji I, Rodriguez P, Manas O, Lensink K, Law M, Kurzman L, et al. A weakly supervised consistency-based learning method for COVID-19 Segmentation in CT images. *Proc 2021 IEEE Winter Conf Appl Comput Vis.* 2021; 2452–2461.
<https://doi.org/10.48550/arXiv.2007.07012>
58. Jia H, Tang H, Ma G, Cai W, Huang H, Zhan L, et al . PSGR: Pixel-wise Sparse Graph Reasoning for COVID-19 Pneumonia Segmentation in CT Images. *arXiv preprint. arXiv:2108.03809*. 2021; 1–10.
<https://doi.org/10.48550/arXiv.2108.03809>
59. Singh VK, Abdel-Nasser M, Pandey N, Puig D. Lunginfseg: Segmenting covid-19 infected regions in lung ct images based on a receptive-field-aware deep learning framework. *Diagnostics*. 2021; 11(2): 158-177
<https://doi.org/10.3390/diagnostics11020158>
60. Chen Y, Zhou T, Chen Y, Feng L, Zheng C, Liu L, et al. HADCNet: Automatic segmentation of COVID-19 infection based on a hybrid attention dense connected network with dilated convolution. *Comput Biol Med* . 2022; 149(July): 105981.
<https://doi.org/10.1016/j.compbimed.2022.105981>
61. Wang X, Yuan Y, Guo D, Huang X, Cui Y, Xia M, et al. SSA-Net: Spatial self-attention network for COVID-19 pneumonia infection segmentation with semi-supervised few-shot learning. *Med Image Anal* .2022; 79: 102459.
<https://doi.org/10.1016/j.media.2022.102459>
62. Owais M, Baek NR, Park KR. DMDF-Net: Dual multiscale dilated fusion network for accurate segmentation of lesions related to COVID-19 in lung radiographic scans. *Expert Syst Appl.* 2022 Sep 15;202. <https://doi.org/10.1016/j.eswa.2022.117360>
63. Jia H, Tang H, Ma G, Cai W, Huang H, Zhan L, et al. A convolutional neural network with pixel-wise sparse graph reasoning for COVID-19 lesion segmentation in CT images. *Comput Biol Med* . 2023; 155: 106698.
<https://doi.org/10.1016/j.compbimed.2023.106698>
64. Fan X, Feng X. SELDNet: Sequenced encoder and lightweight decoder network for COVID-19 infection region segmentation. *Displays*. 2023; 77(January): 102395. <https://doi.org/10.1016/j.displa.2023.102395>
65. Peng Y, Zhang T, Guo Y. Cov-TransNet: Dual branch fusion network with transformer for COVID-19 infection segmentation. *Biomed Signal Process Control*. 2023; 80.
<https://doi.org/10.1016/j.bspc.2022.104366>

ECGANCOVID: بنية شبكة الخصومة التوليدية المشروطة الفعالة لتجزئة مرض كوفيد-19

بيمان حسين حسن^{1,2} ، أ.د. اسراء هادي علي¹

¹قسم البرمجيات، كلية تكنولوجيا المعلومات، جامعة بابل ، بابل، العراق.
²قسم تقنيات أنظمة الحاسوب، المعهد التقني بابل، جامعة الفرات الاوسط التقنية، كوفة، العراق.

الخلاصة

تشكل متلازمة الجهاز التنفسي الحادة الوبائية فيروس كورونا 2 (SARS-CoV-2) تهديدًا عالميًا، مما يؤثر على الملايين في جميع أنحاء العالم. في حين أن الكشف الآلي عن التهابات الرئة من خلال التصوير المقطعي المحوسب (CT) يعد بديلاً واعدًا، فإن تجزئة المناطق المصابة من شرائح الأشعة المقطعية لا تزال صعبة بسبب حدود العدوى منخفضة التباين والمظاهر غير الواضحة. ولمواجهة هذا التحدي، تم اقتراح نموذج للتعلم العميق يسمى ECGANCOVID-Net للكشف عن المناطق المصابة وتحديدتها في الصور المقطعية للصدر. يستخدم نموذجنا أداة القطع الهرمي الدلالي للكشف عن مناطق عدوى الرئة الناجمة عن فيروس كورونا في الصور الطبية المقطعية. ويتكون النموذج من عنصرين، هما نماذج U-CGAN-Net. تم تصميم الشبكة العصبية الأولية، UCGAN-Net1، للكشف عن حمة الرئة. وبعد ذلك، تعمل الشبكة العصبية الثانية، UCGAN-Net 2، على الرئتين المجزأتين لتحديد المناطق المحددة المتأثرة بأفات كوفيد-19 بدقة. تتكون شبكة UCGAN-Net من شبكة الخصومة التوليدية المشروطة (CGAN) التي تتضمن مولدًا ومميزًا مُكَيَّفًا. بالإضافة إلى ذلك، يستخدم نموذجنا تقنيات زيادة البيانات لمعالجة مسألة بيانات التدريب المحدودة. ومن خلال التجارب المكثفة، تم اكتشاف أن المنهجية المقترحة تظهر أداءً متفوقًا مقارنة بالتقنيات المقترحة مؤخرًا. ويتجلى هذا بشكل خاص في الأداء العام المحسن لنموذجنا عند التحديد الدقيق لموقع الآفات الصغيرة. أظهرت شبكة ECGANCOVID المقترحة أداءً استثنائيًا في تجزئة آفات كوفيد-19، وحققت أداء توطين أعلى مع معامل تشابه النرد (DSC) بنسبة 84.5% والتقاطع عبر الاتحاد (IOU). بالإضافة إلى ذلك، خضع النموذج المقترح للتحقق الخارجي باستخدام مجموعة البيانات الغير مرئية، مما أدى إلى معامل تشابه النرد بنسبة 69.7%.

الكلمات المفتاحية: مرض كوفيد-19 ، صور التصوير المقطعي المحوسب ، شبكة الخصومة التوليدية الشرطية (CGAN)، تجزئة الرئة والآفات، ستراتيجية التقسيم الهرمية.